Distributions of pore sizes and atomic densities in binary LJ glasses revealed by molecular dynamics simulations

[1]Nikolai Priezjev and [2]Maxim Makeev

[1]Department of Mechanical Engeneering

Wright State University

[2]Department of Chemistry

University of Missouri-Columbia

APS March Meeting 2018, March 07 2018

Outline

We report on the results of a molecular dynamics simulation study of binodal glassy systems formed in the process of isochoric rapid quenching from a high-temperature fluid phase. The transition to vitreous state occurs due to concurrent spinodal decomposition and solidification of the matter. The study is focused on topographies of the porous solid structures and their dependence on temperature and average density. To quantify the pore-size distributions, we put forth a scaling relation that provides a robust data collapse in systems with high porosity. We also find that the local density of glassy phases is broadly distributed, and, with increasing average glass density, a distinct peak in the local density distribution is displaced toward higher values.

Porous glasses: Structure and length-scales

Structure of different open-cell polymeric foams (1a, 2a) and the respective porous glass replicates after calcination (1b,2b).

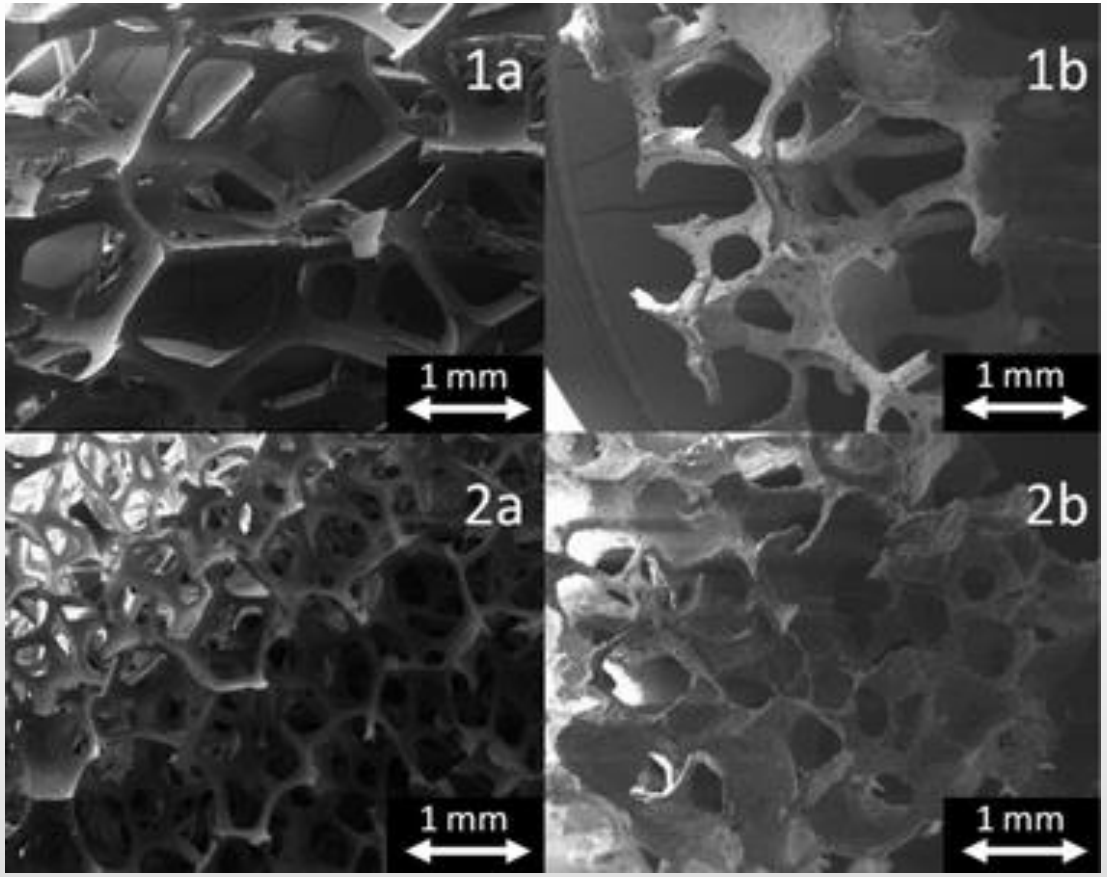

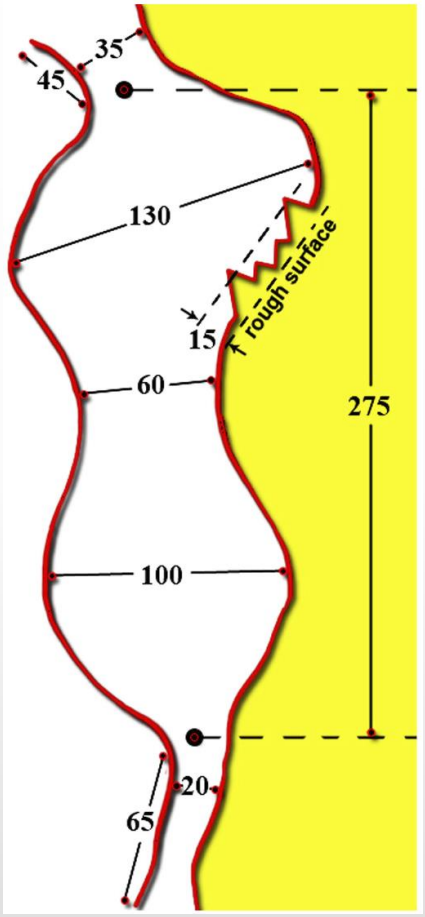

A. C. Mitropoulos, K. L. Stefanopoulos, E. P. Favvas, E. Vansant, and N. P. Hankins, Sci. Rep. **5**, 10943 (2015).

Porous glasses. Aspects of Structure & Topography

Sodium borosilicate glass – Experiment

Three-dimensional reconstruction of a sodium borosilicate glass monolith

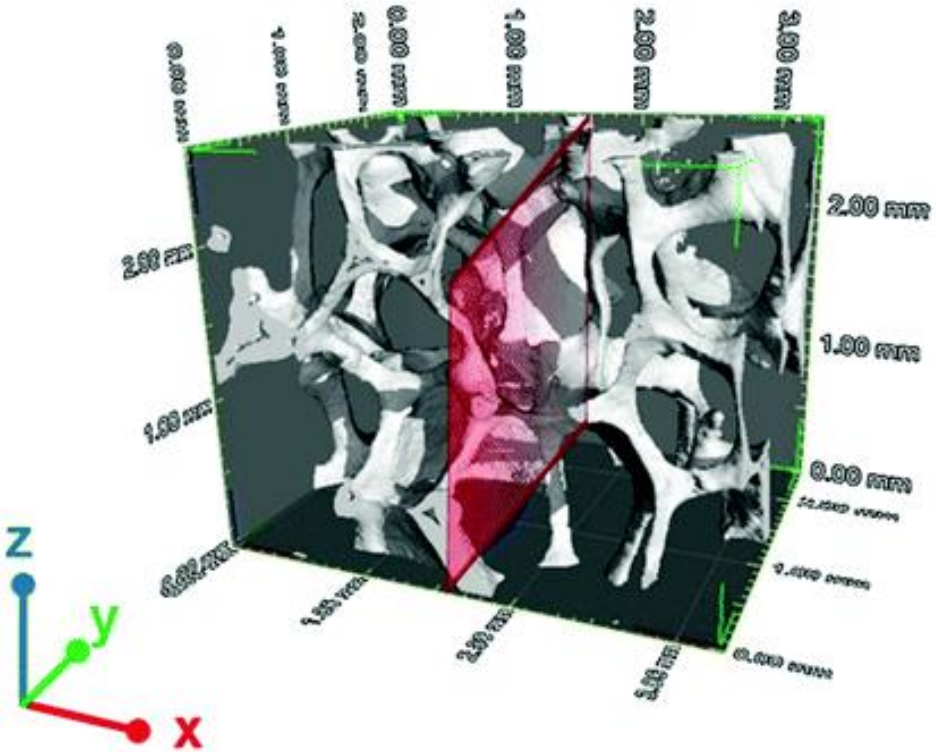

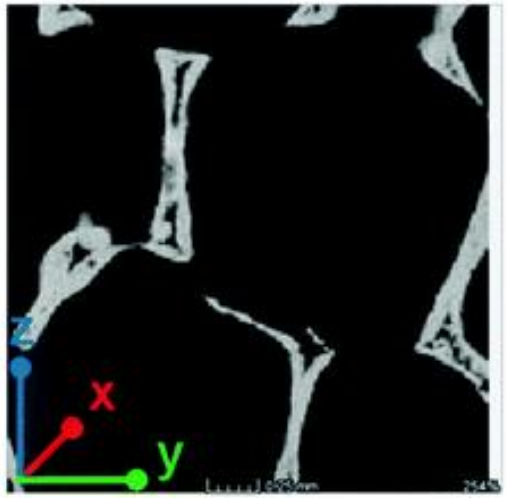

Borosilicate glass is a type of glass with silica and boron trioxide as the main glass-forming constituents.

B. Reinhardt, J. Herwig, S. Rannabauer, M. Scheffler and D. Enke, J. Eur. Ceram. Soc. **34**, 1465 (2014).

Theoretical Model

Kob-Andersen Model

composed of 80% large particles (A) and 20% smaller particles (B)

Metallic glass (homologous to the $Ni_{80}P_{20}$ metal alloy)

$$V(r) = 4\varepsilon_{\alpha\beta}\left[\left(\sigma_{\alpha\beta}/r\right)^{12} - \left(\sigma_{\alpha\beta}/r\right)^{6}\right]$$

$$\alpha, \beta \in \{A, B\}$$

$$R_{cut} = 2.5\sigma_{\alpha\beta}$$

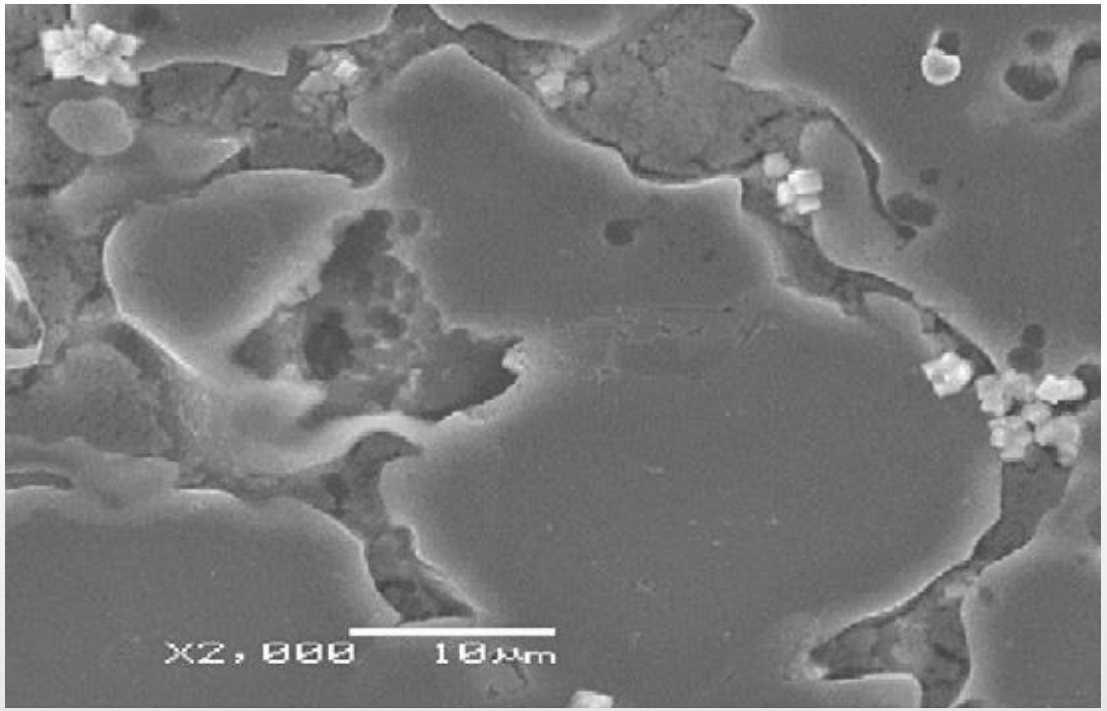

$$\sigma_{AA} = \sigma; \sigma_{BB} = 0.8\sigma;\ \sigma_{BB} = 0.88\sigma;\ \epsilon_{AA} = \varepsilon;\ \varepsilon_{AB} = 1.5\varepsilon;\ \varepsilon_{BB} = 0.5\varepsilon$$

W. Kob and H. C. Andersen, Phys. Rev. E **51**, 4626 (1995).

Theoretical Model: Lennard-Jones Systems

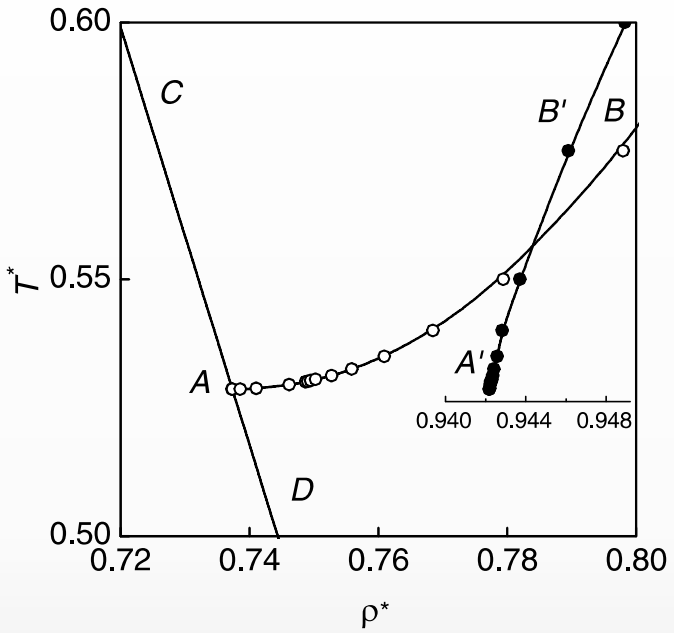

Systems of Lennard-Jones particles is used to determine the spinodal of a stretched liquid and crystal and the lines of their phase equilibrium at negative pressures.

The boundary of the thermodynamic stability of a homogeneous phase (*spinodal*) is determined by the condition: $\left(\frac{\partial p}{\partial \rho}\right)_T = 0$

(T, ρ) projection of the spinodal (CD) and the line of liquid-crystal equilibrium (AB, A'B').

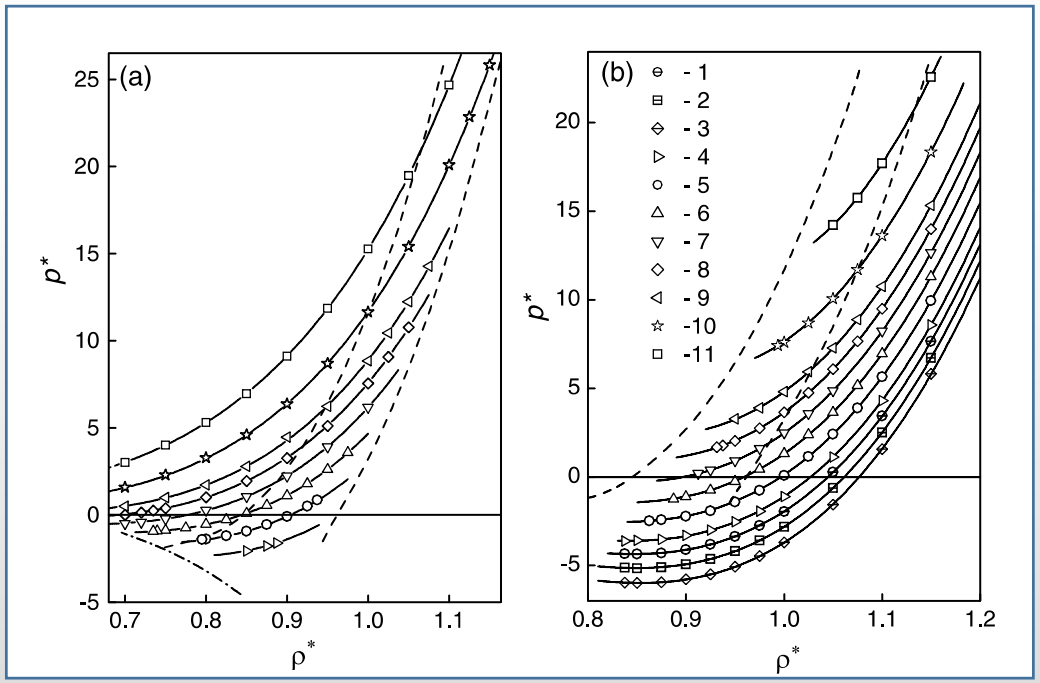

Crystalline phase: $p^* = \sum_{n=0}^{N} \sum_{m=0}^{M} a_{nm} \rho^{*n} T^m$

V. G. Baidakov and S. P. Protsenko, Phys. Rev. Lett. **95**, 015701 (2005).

Theoretical Model: Surface Energy

Surface Energy: $\gamma = \frac{1}{2}\int_{-L/2}^{+L/2}[p_n(z) - p_t(z)]dz$

Correction to the surface energy:

$$\gamma_{cor} = 12\pi(\rho_{liq} - \rho_{gas})^2 \times \int_0^1 ds \int_{r_c}^{\infty} dr\, r^{-3}(3s^3 - s)coth\left(\frac{2sr}{\xi}\right)$$

Density variation at the interface:

$$\rho(z) = \frac{1}{2}(\rho_{liq} - \rho_{gas}) - \frac{1}{2}(\rho_{liq} - \rho_{gas})\tanh\left(\frac{2(z-z_0)}{\xi}\right)$$

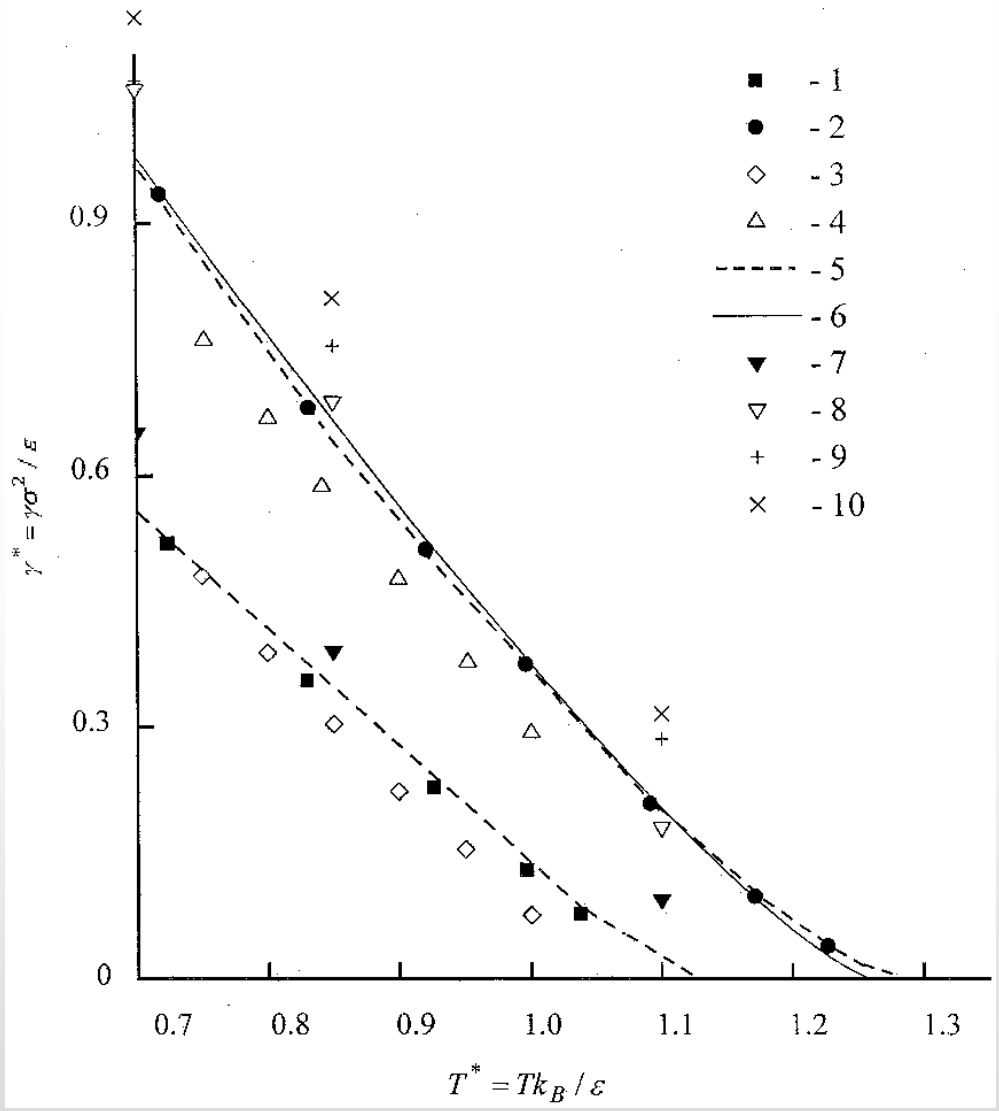

V. G. Baidakov, G. G. Chernykh, and S. P. Protsenko, Chem. Phys. Lett. **321**, 315 (2000).

Theoretical Model: *Modus Operandi*

Kob-Andersen Model of glass

$T_g = 0.435\ \varepsilon/k_B$

W. Kob and H. C. Andersen, Phys. Rev. Lett. **73**, 1376 (1994).

High-temperature fluid

⇩

Equilibration: $3\times10^4\ \tau$

⇩

Cooling to T = 0.02-0.2 ε/k_B

⇩

Relaxation at constant T ($3\times10^4\ \tau$)

Phase Separation

I. M. Lifshitz and V. V. Slezov, Sov. Phys. JETP **35(8)**, 331-339 (1959).

- Kinetics of phase separation is complex
- Strong dependence on both: T and ρ
- Possible logarithmic corrections

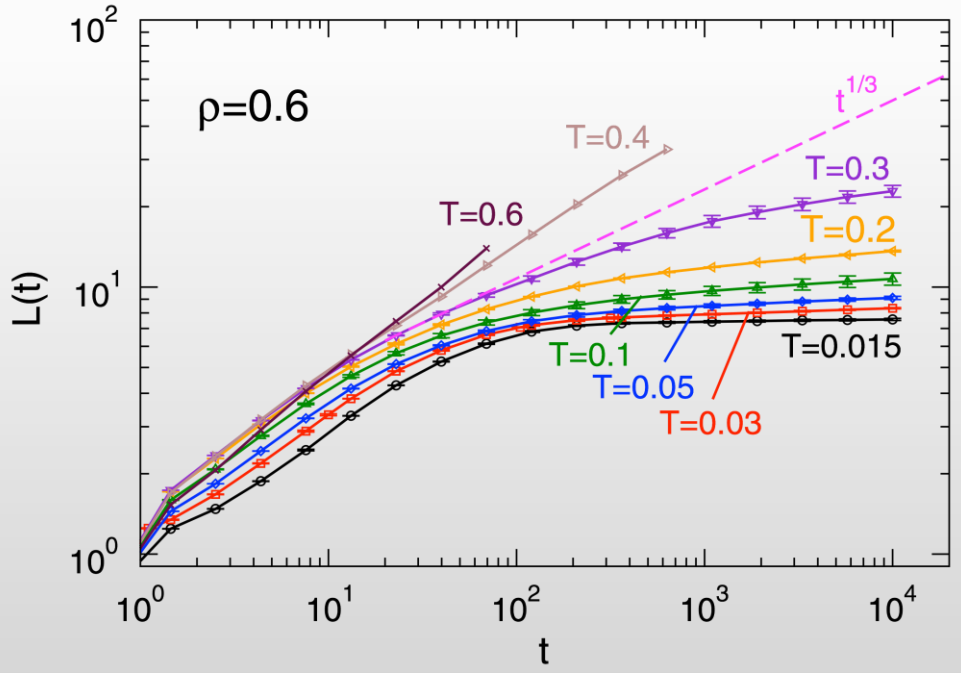

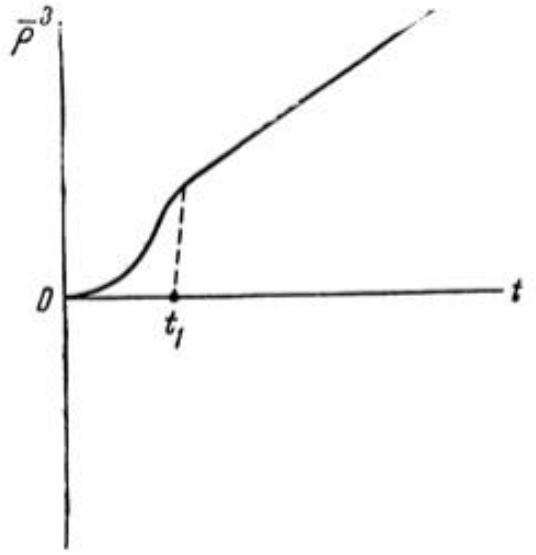

Phase Separation: Dynamics. I

Dynamical evolution of the binary system with $\rho = 0.3$. Illustrates the void-space nucleation and evolution.

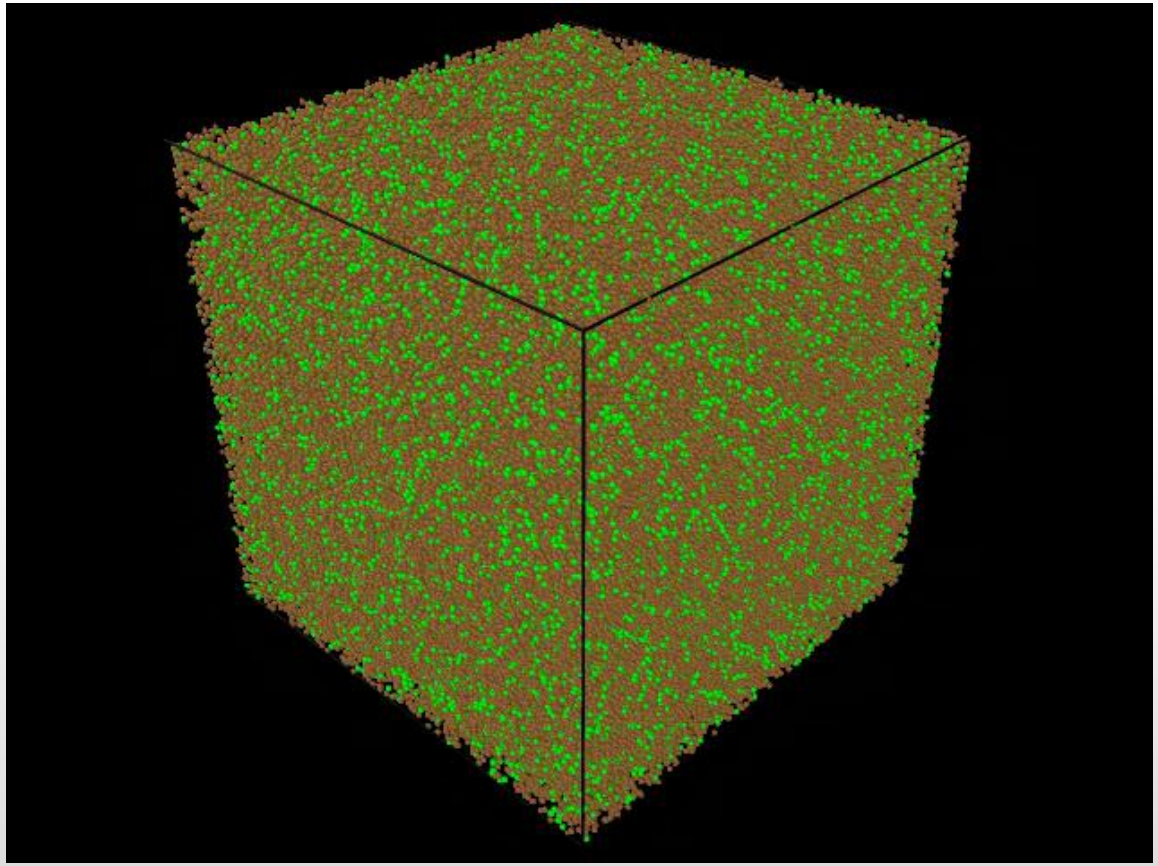

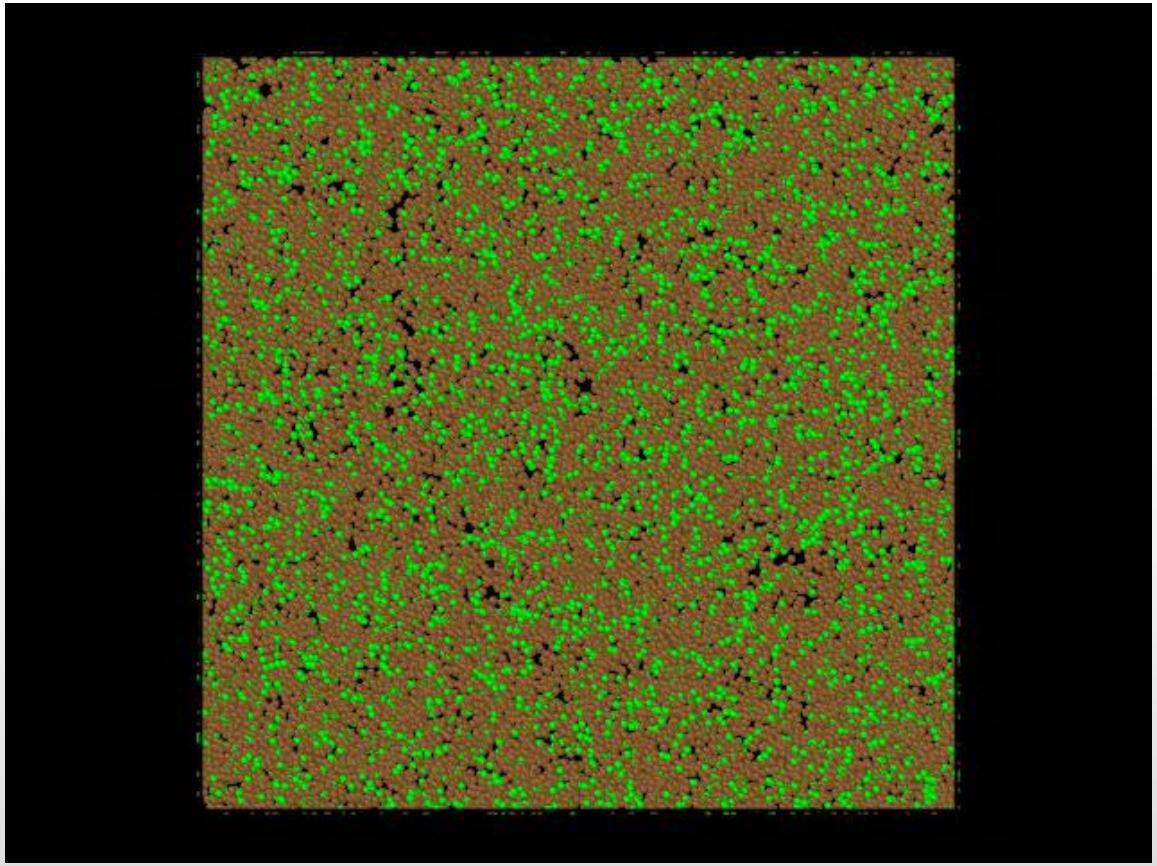

Phase Separation: Dynamics. II

Dynamical evolution of the binary system with $\rho = 0.4$. Illustrates the void-space nucleation and evolution.

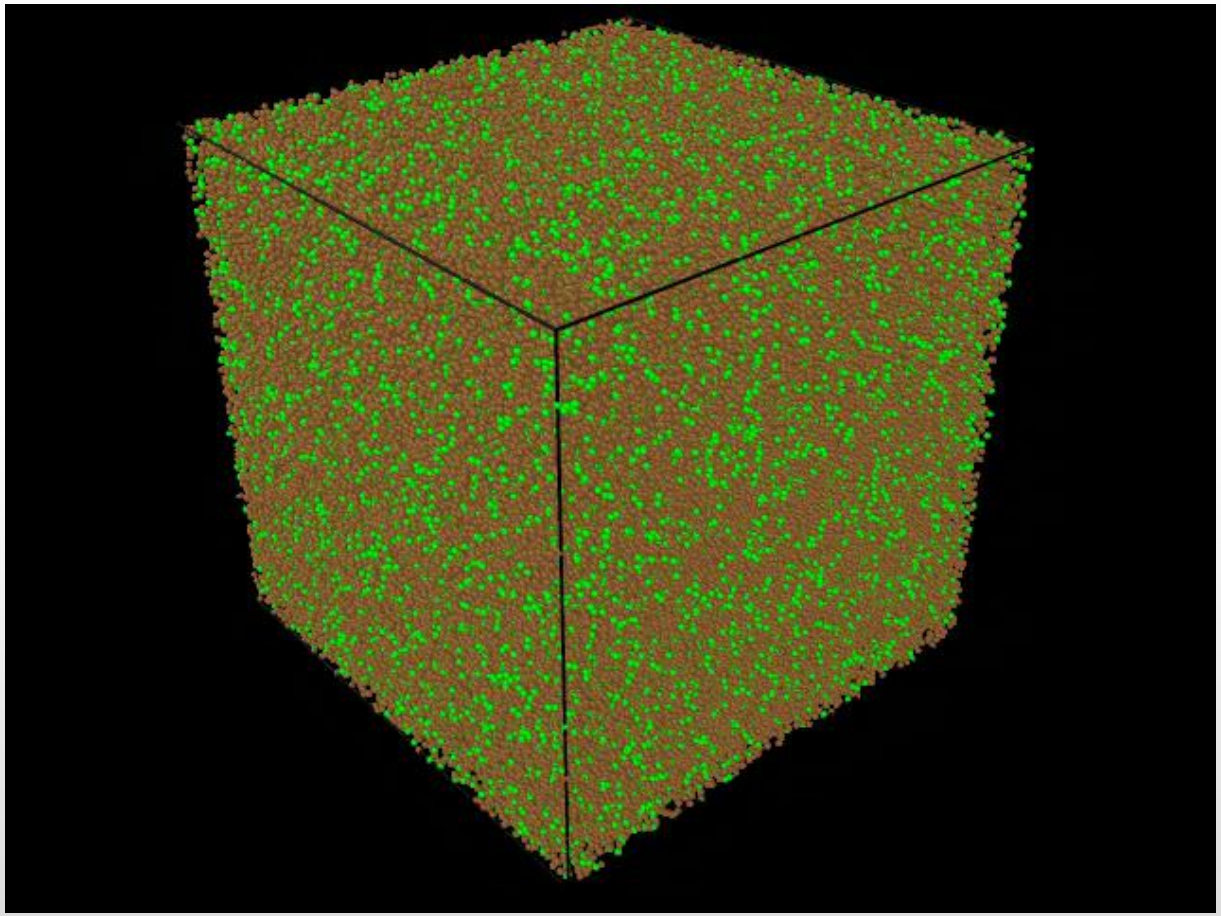

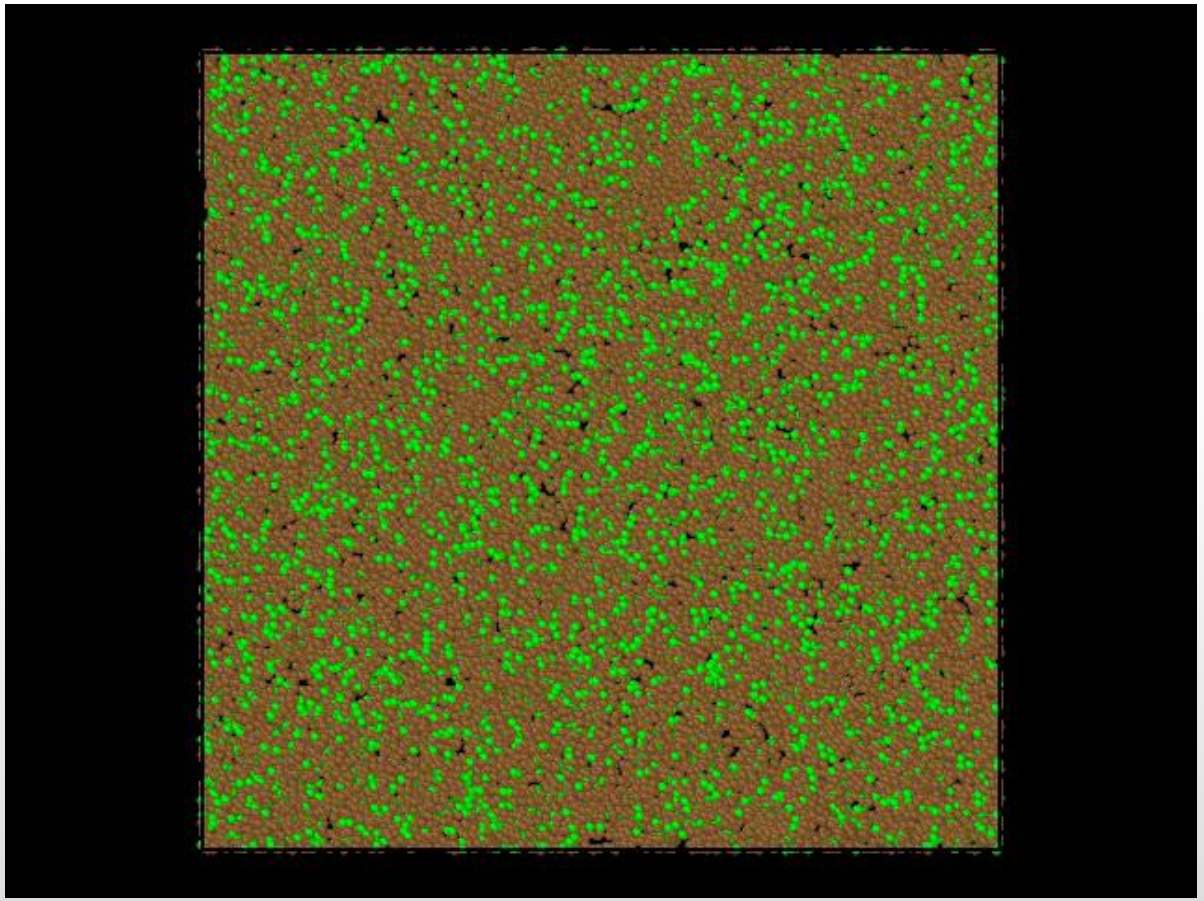

On the driving force of phase separation

Pressure dependence on temperature (reduced units), measured in systems with different $\rho\sigma^3$.

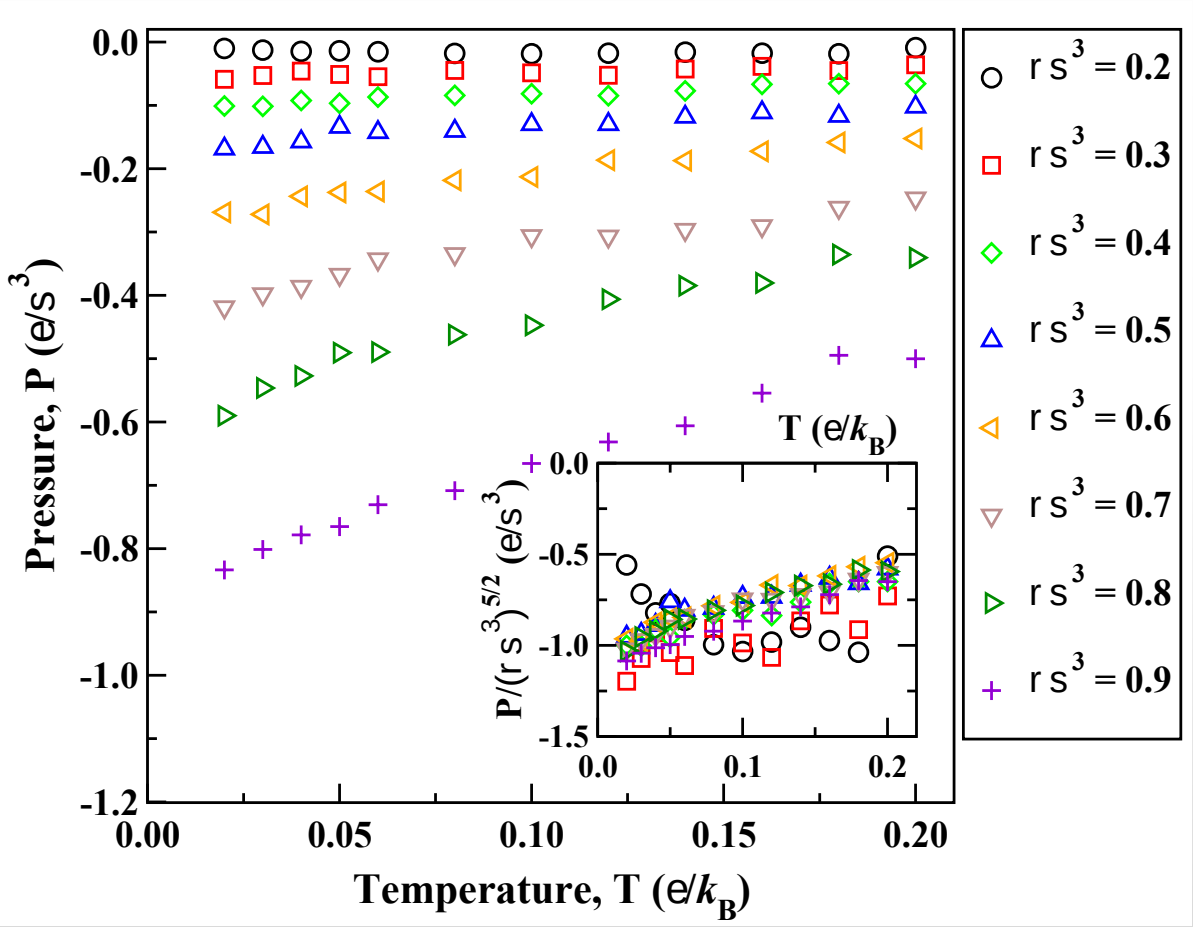

Pressure versus temperature dependence at different densities obeys the following scaling relation:

$$\frac{P}{T} \sim \rho^{5/2}$$

- **The phase separation takes place under negative pressure, which relaxes depending on T**
- **The effective confinement introduced barriers**
- **The evolution occurs such that derivative of pressure with respect to local density is negative**
- **Density suppresses diffusivity and prolongs relaxation**

Pore-size distribution functions

Pore-size (diameter) distribution functions are plotted at three characteristic densities, $\rho\sigma^3$: 0.2; 0.5, 0.7, 0.9.

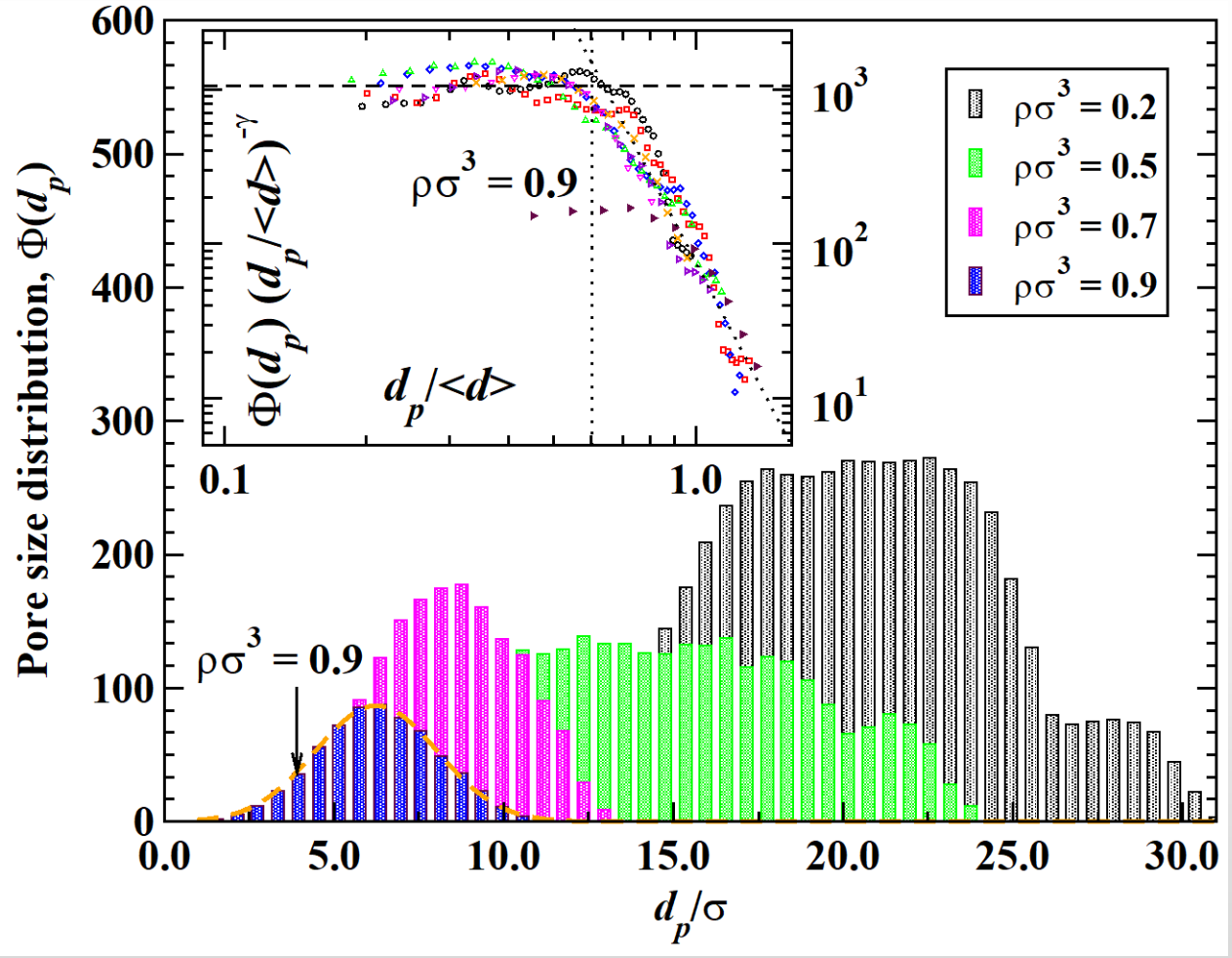

In the range of small and intermediate values of dp, the PSDs obey the following scaling relation:

$$\Phi(d_p) \sim (d_p/\langle d\rangle)^{\gamma} \mathrm{f}(d_p/\langle d\rangle)$$

- **Scaling holds for systems with $\rho\sigma^3$ smaller than the bulk density**
- **In the limit of large d_p values, a peak is observed**
- **The peak magnitude is an increasing function temperature**
- **The behavior is somewhat similar to the PSD measured in experimental studies**
- **The experimental peaks are close in magnitude to the peak in the region of small d_p**

Pore-size distribution functions: Bulk limit

- Scaling break down at densities close to the bulk value
- Pore-size distribution shows a Gaussian shape
- Pore-size distributions are narrow
- Voids dimensions are close to atomic scales

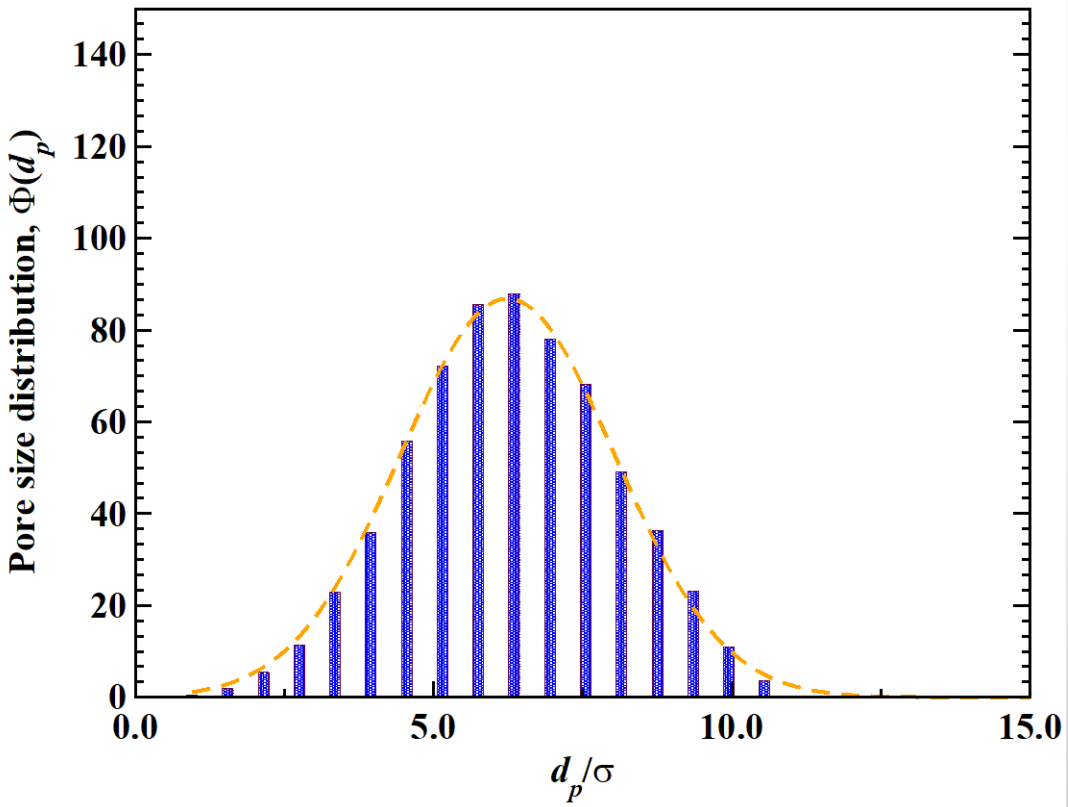

Not an artifact

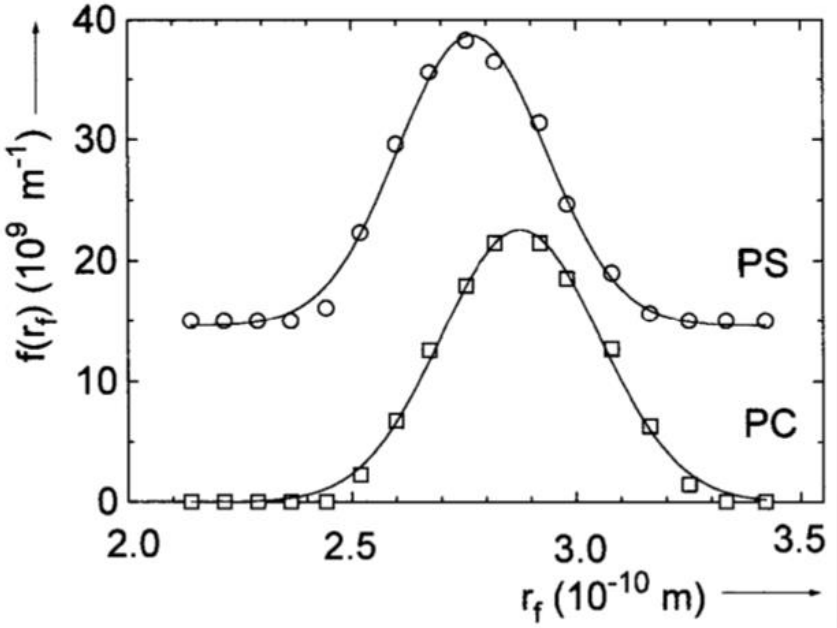

- **Free volume hole radius density distribution $f(r_f)$ in glassy polycarbonate (PC) and polystyrene (PS).**
- **The solid curves in the figure shows two Gaussians fitted to the experimental data.**

G. Dlubek, A. P. Clarke, H. M. Fretwell, S. B. Dugdale, and M. A. Alam, phys. stat. sol. (a) **157**, 351 (1996).

Temperature dependence

- Maximum pore size is sensitive to temperature
- Different regimes in temperature dependence
- Strong dependence on density

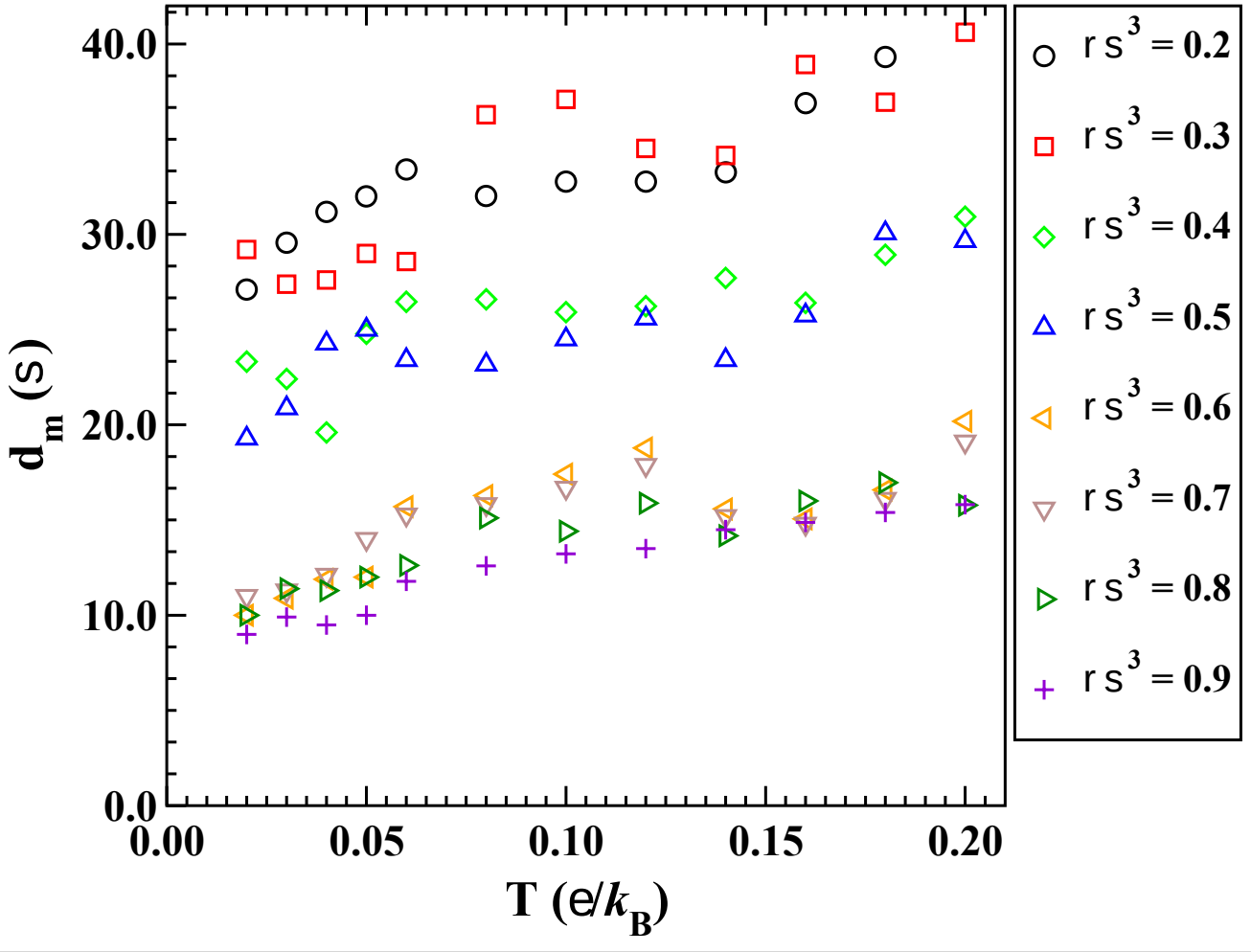

- Shape is largely preserved
- Peak at large pore sizes is sensitive to T
- Piecewise dependence on average density
- Three distinct regimes in density
- The shapes of curves possess similar features
- Increments are of the same order

Local density: Theory

$L \subset \mathbb{R}^3$

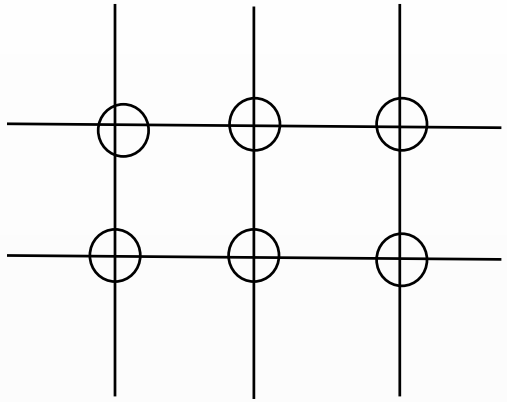

Closed ball

$$B_R = \left\{ R \in \mathbb{R}^3 : \sum_{j=1}^{3} R_j^2 < R_0^2 \right\}$$

Average density

$$\langle \rho \rangle = (1/V) \sum_{i=1}^{N} \delta(\vec{r}_i) = \frac{N}{V} = \rho\sigma^3$$

Average local density

$$\langle \rho \rangle_B = (1/B_R) \int dR^3 \, \delta\left(\vec{r}_i - \vec{R}_i\right)$$

- Average local density can be can be regarded as a measure of deviation of the local density from the average density of homogeneous dense system.
- Average local density of a homogeneous sample is constant for R_0 above its threshold value

Local density of solid domains

$\rho\sigma^3$: a) 0.2; b) 0.3; c) 0.4; d) 0.5; e) 0.6; f) 0.7; g) 0.8; h) 0.9; i) 1.0

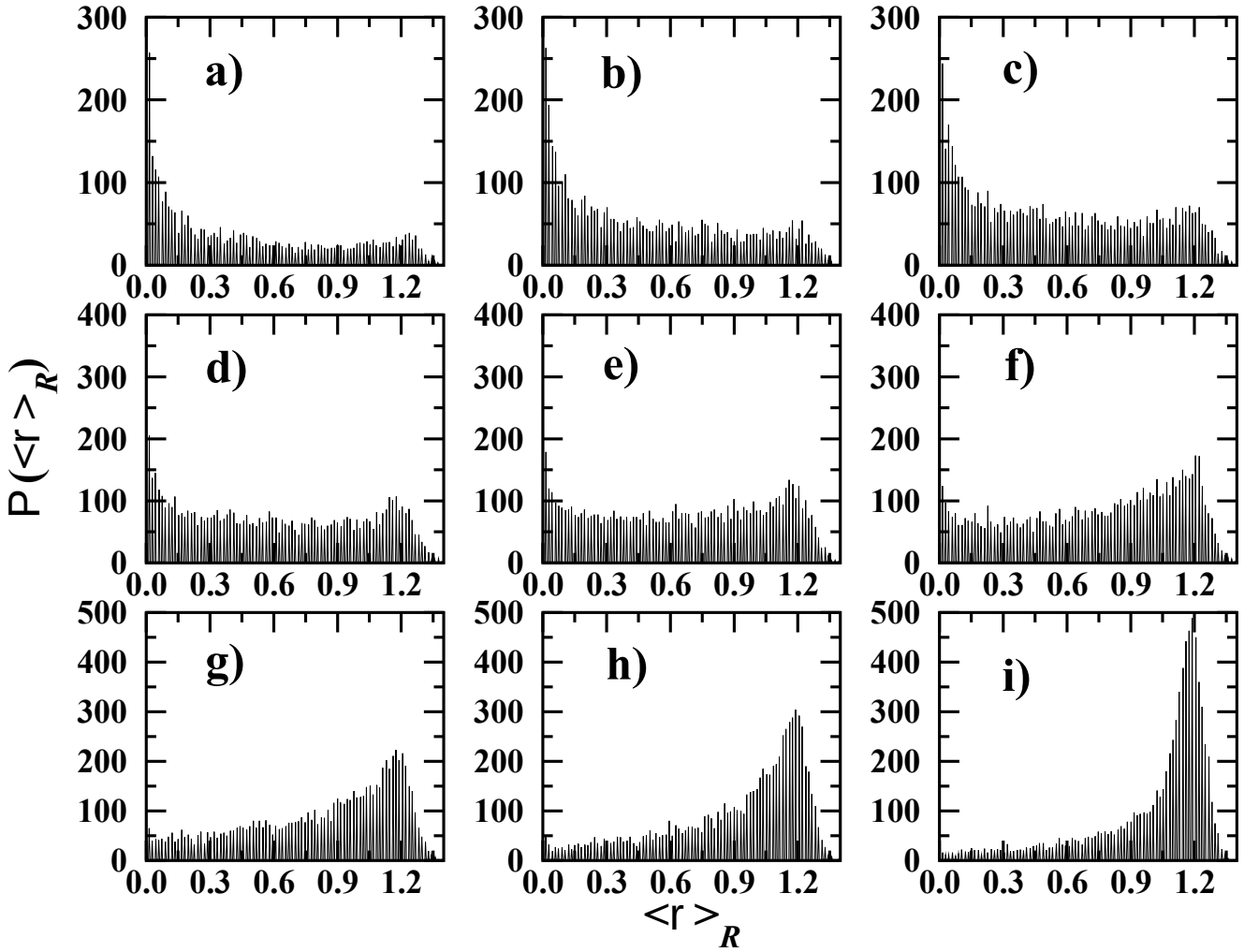

- Solid domain correspond to density at around 1.2
- The maximum local density is larger for small values of $\rho\sigma^3$
- Thin solid domains can be more dense than the bulk material with low porosity.
- Implications for mechanics

Local density and porosity

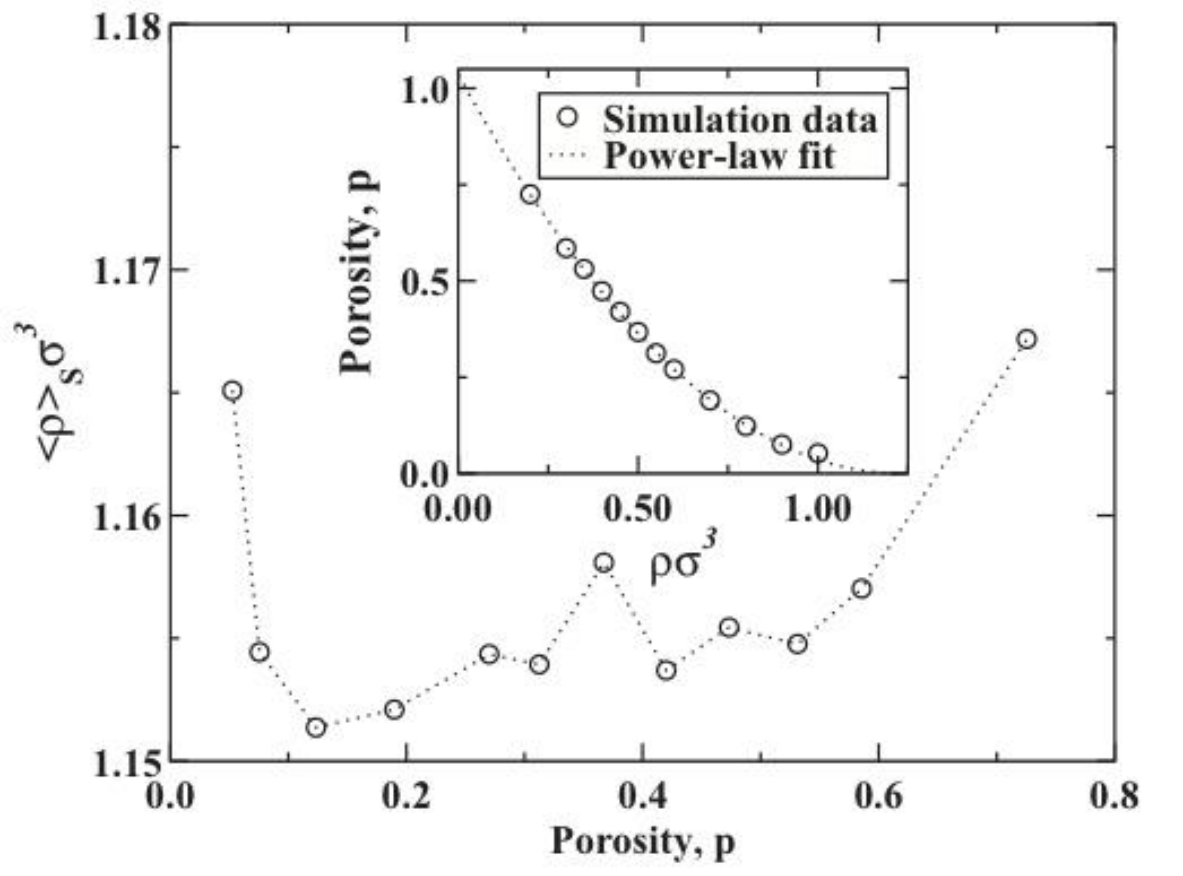

- Local density increases with porosity
- Local density can be higher then average density of bulk glasses
- Implications for mechanical response
- Possibility to maximize the density of solid domains by tuning procedure

Porosity versus average density:

$$p = \left(p_c\sigma^3 - p\sigma^3\right)^{\gamma}$$

$p_c\sigma^3$ - the critical density below which LJ systems develop voids: 1.24

M. A. Makeev and N. V. Priezjev, Phys. Rev. E **97**, 023002 (2018).

Mechanics of porous systems

- Wide range of porosity variation
- Pore response to mechanical loadings:
- Shear loadings
- Compression
- Tension

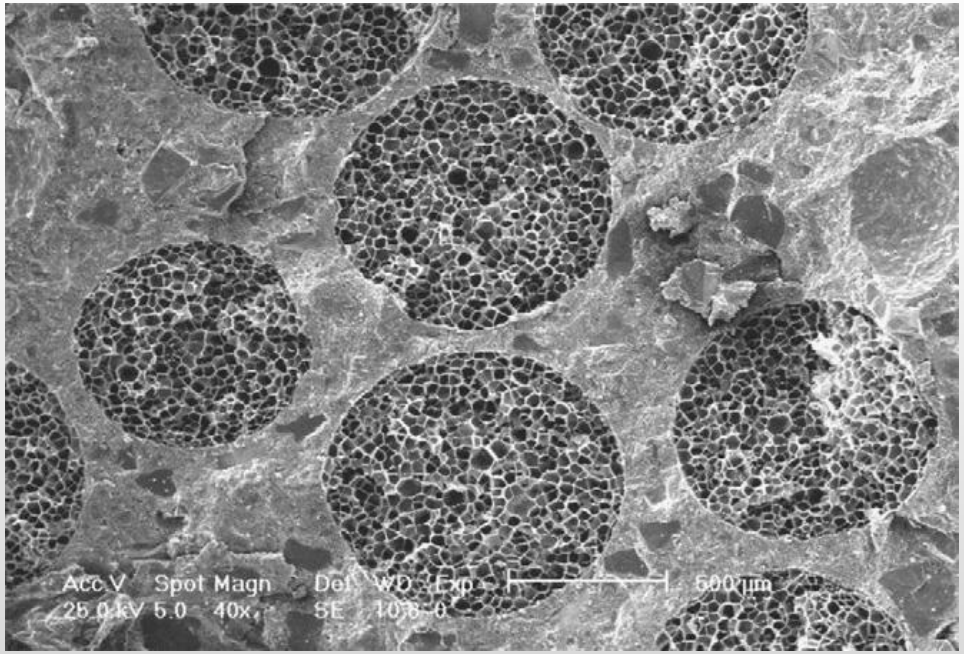

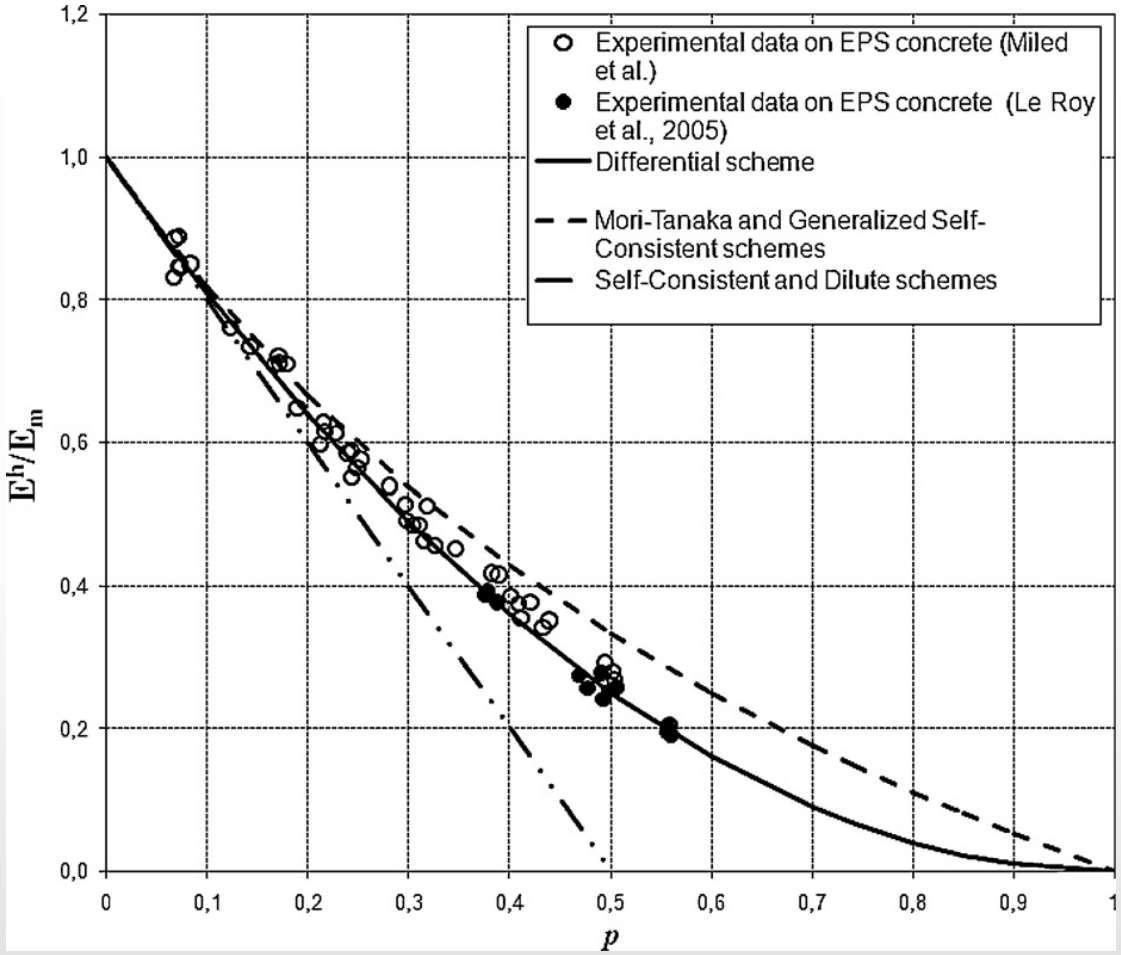

Young modulus of the EPS concrete versus porosity, *p*.

Mechanics of porous systems: Theories. I

Models of elastic response of materials with porosity (p)

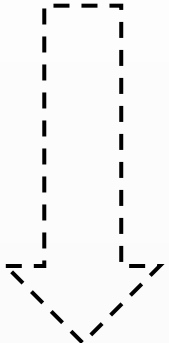

- The dilute or Eshelby method
- the mean-field homogenization method
- the Mori-Tanaka model
- the generalized self-consistent model
- he differential method
- Modifications/extensions of the above

$$\frac{B(p)}{B_m} = \frac{\mu(p)}{\mu_m} = 1 - \theta p$$

$$\frac{B(p)}{B_m} = \frac{\mu(p)}{\mu_m} = \frac{1-p}{1+\theta p}$$

$$\frac{B(p)}{B_m} = \frac{\mu(p)}{\mu_m} = (1 - \theta p)^2$$

Mechanics of porous systems: Theories. II

- Theories does not work over the whole range of p
- Differential method: small and intermediate p
- Large p: percolation theory-based method

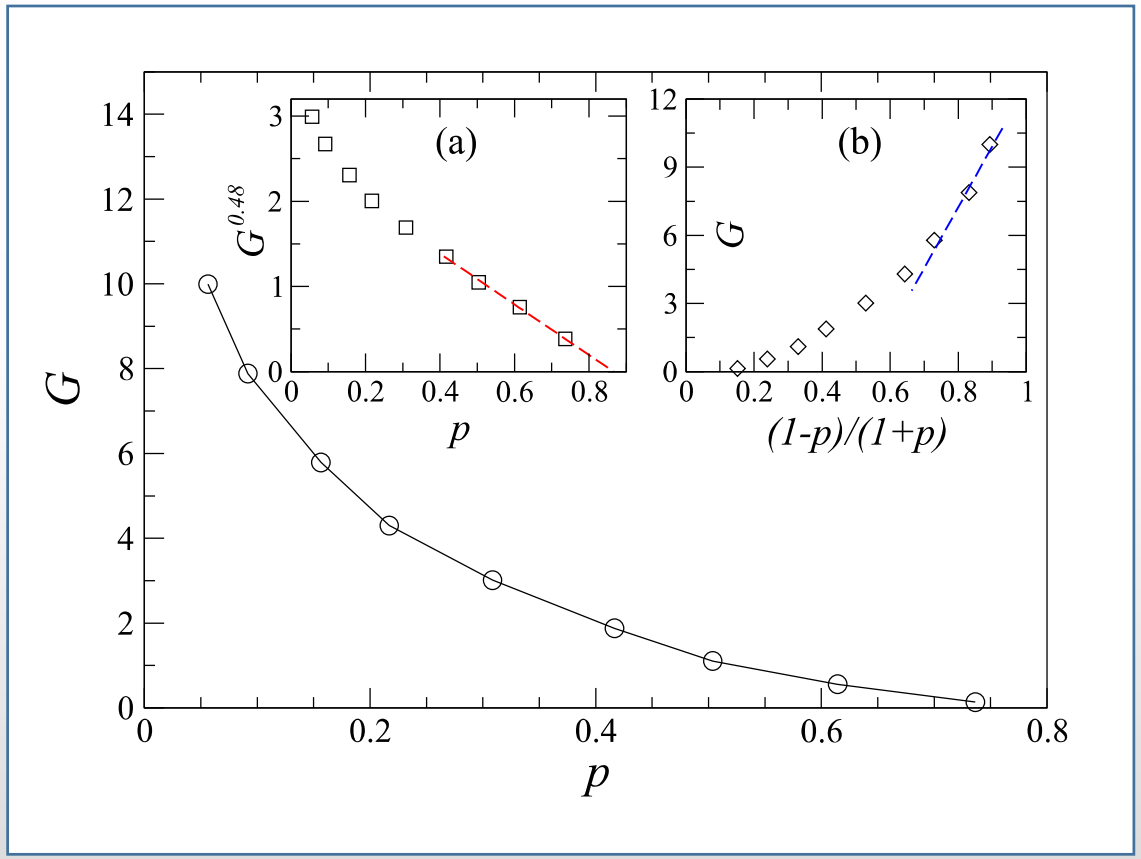

N. V. Priezjev and M. A. Makeev, Phys. Rev. E. **96**, 053004 (2017).

Large porosity limit:

$$G \sim (p_c - p)^{\alpha}$$

$\alpha = 2.1$ *and* p_c=0.87

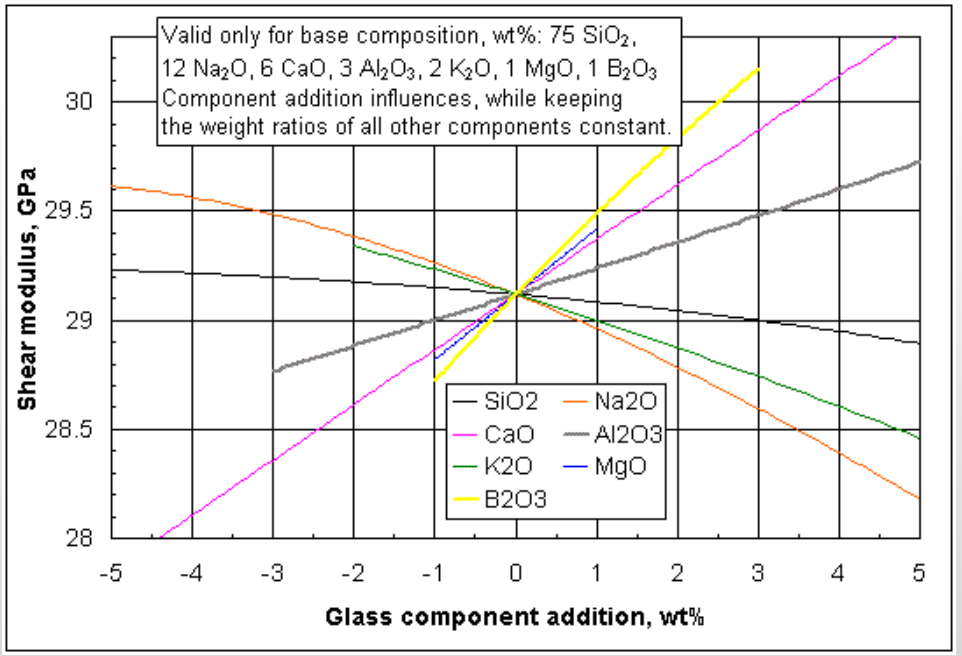

Shearing of porous systems: Illustration

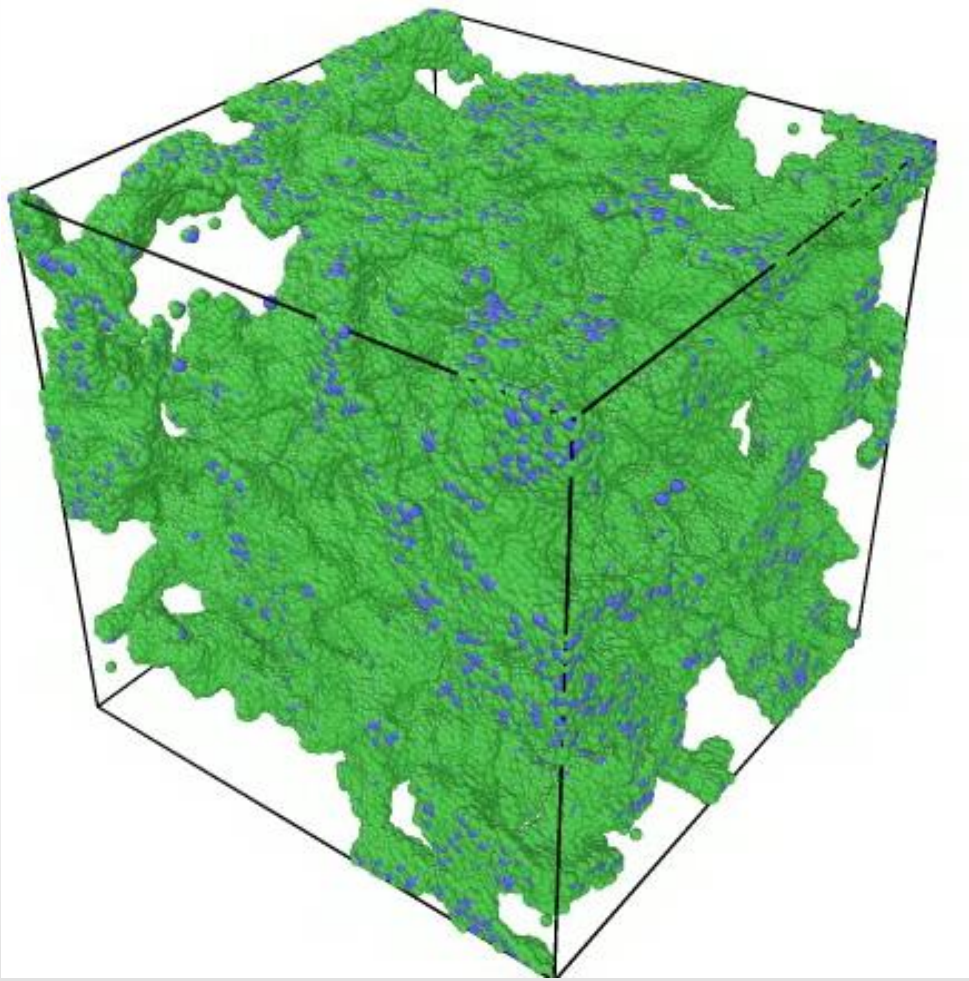

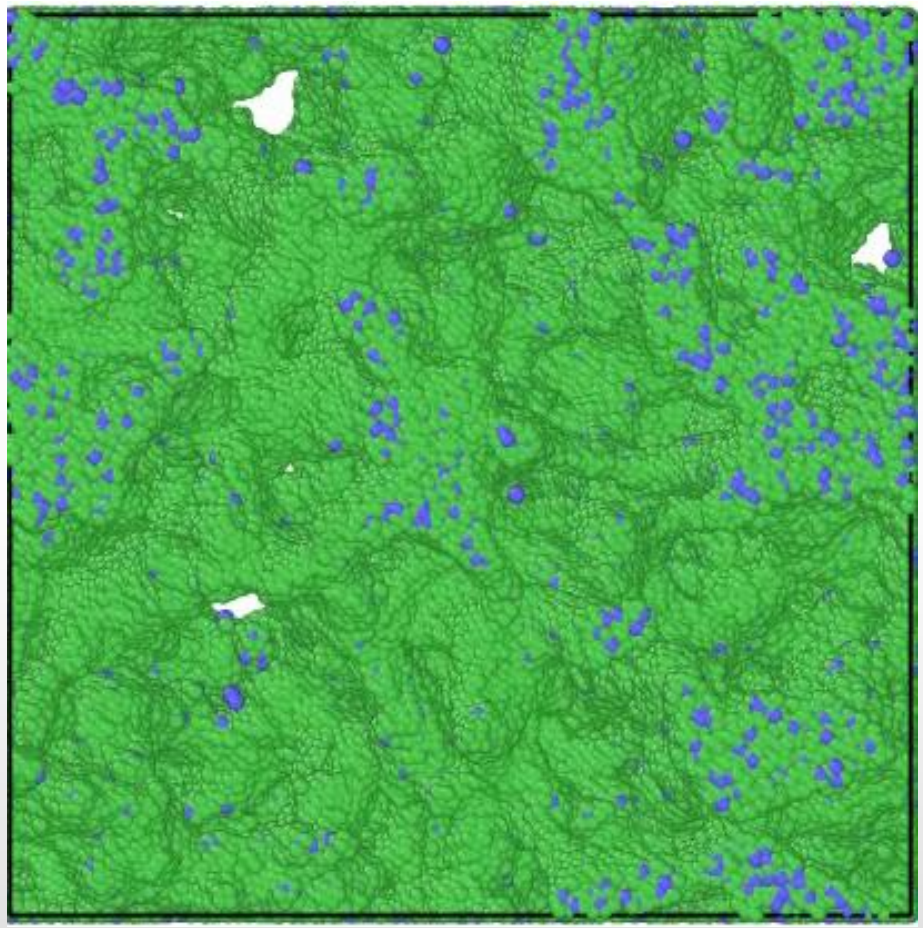

N. V. Priezjev and M. A. Makeev, Phys. Rev. E. **96**, 053004 (2017).

Pore geometry evolution under shear. I

Initial stages of shear loading

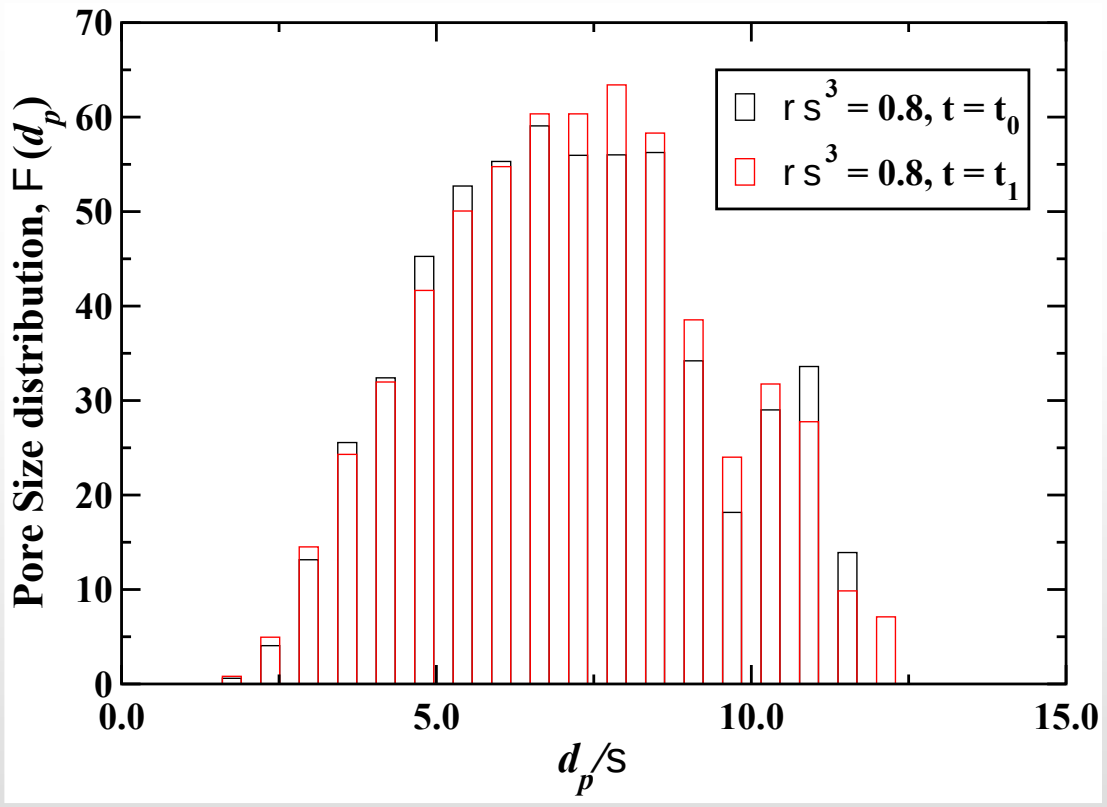

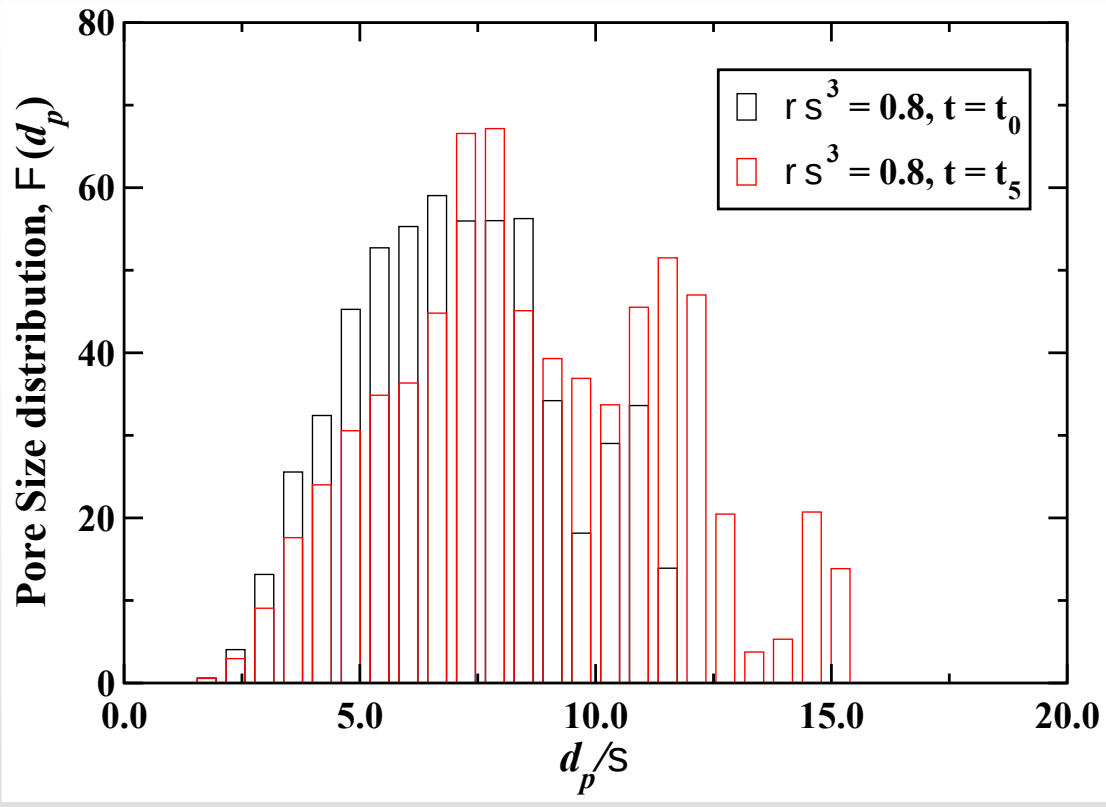

Pore geometry evolution under shear. II

Final stages of shear loading

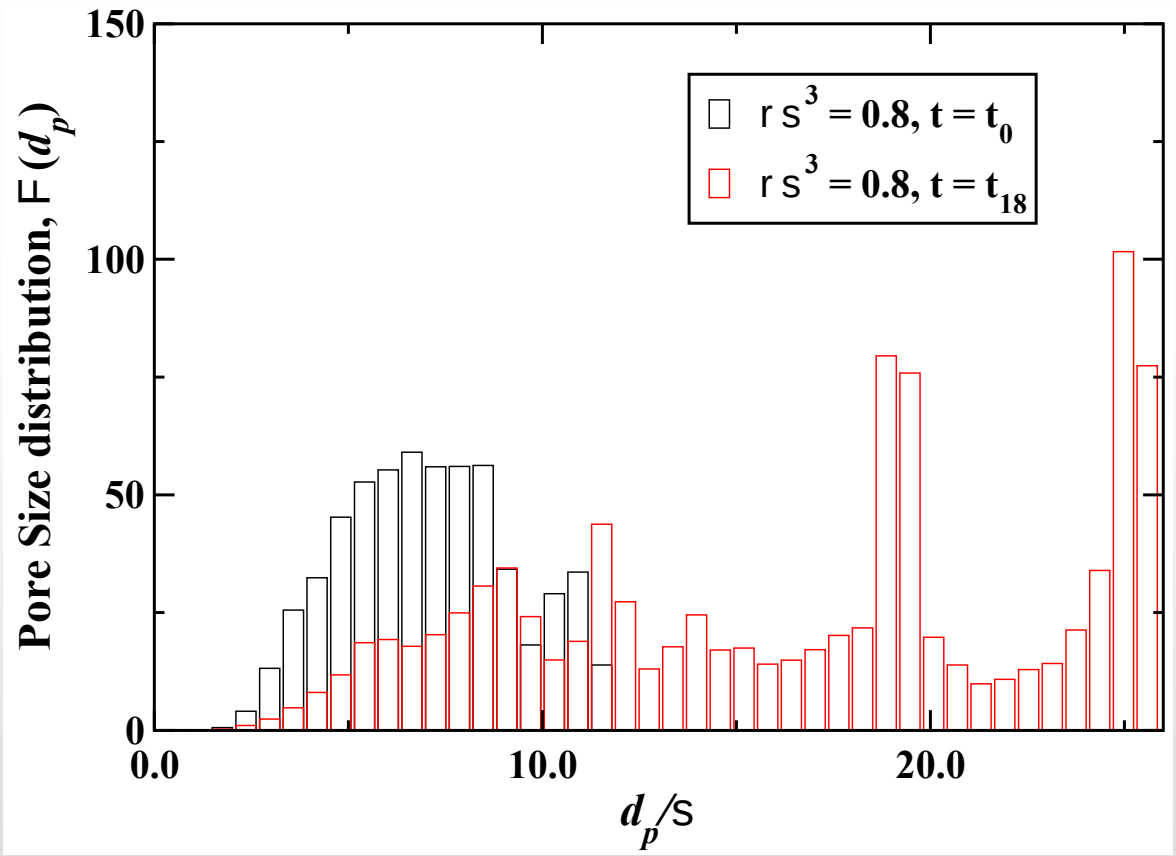

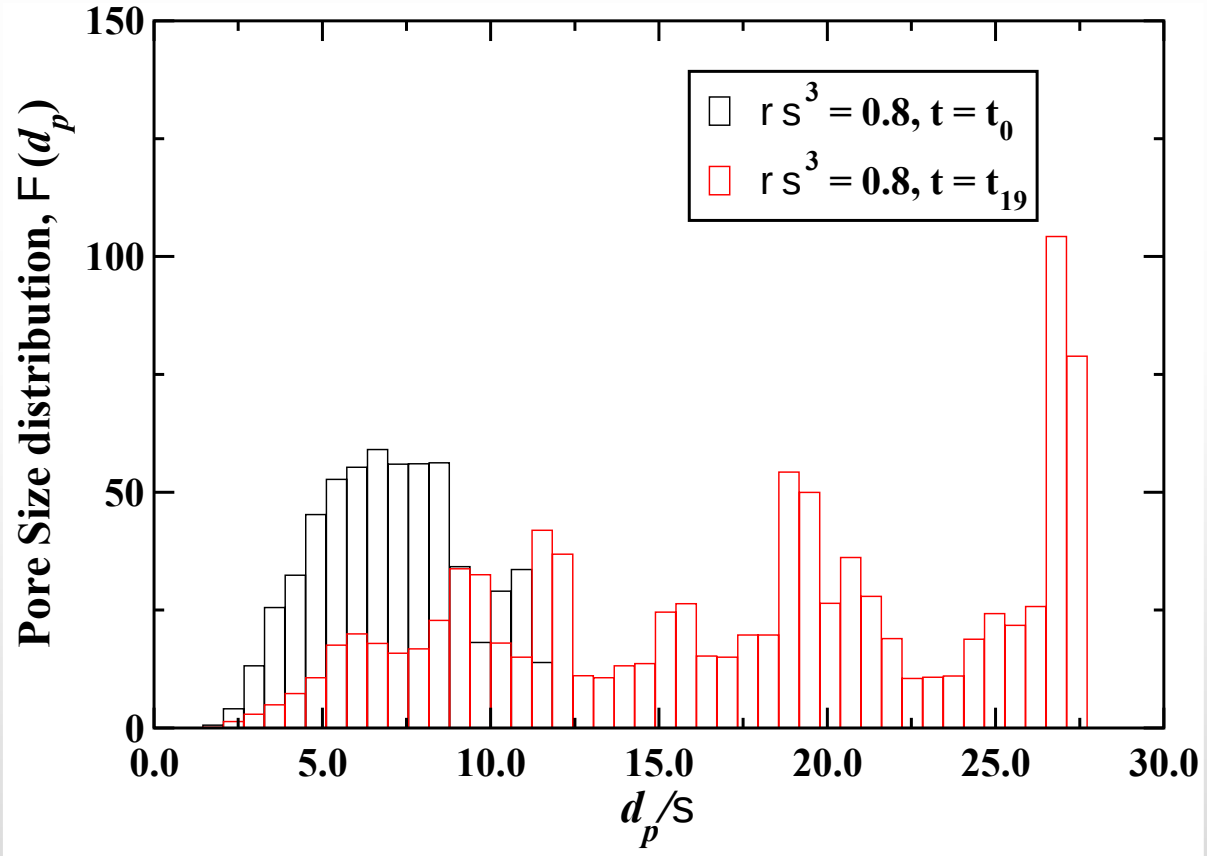

Pore geometry evolution under shear: PSDs

Pore size distributions, measured at $\rho\sigma^3$ = 0.3 (a), 0.5 (b), and 0.8 (c) are shown at different shear strains.

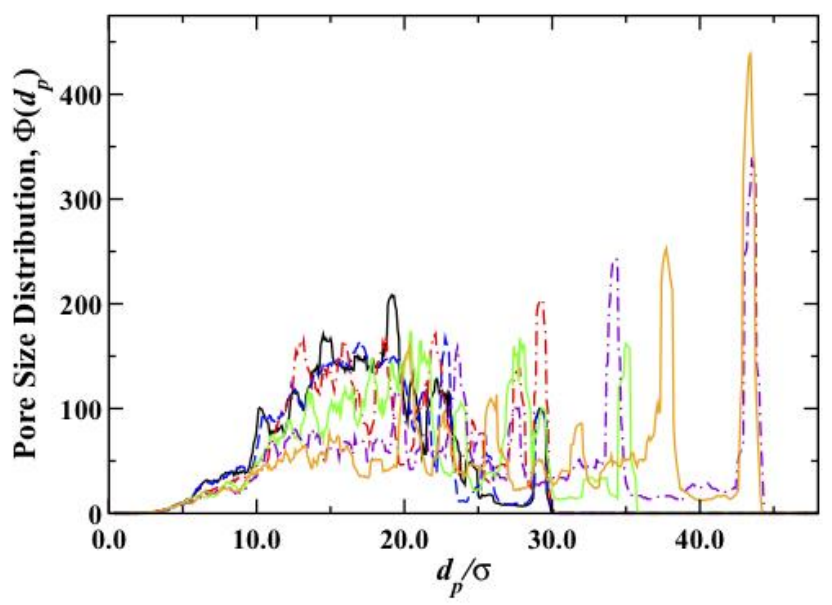

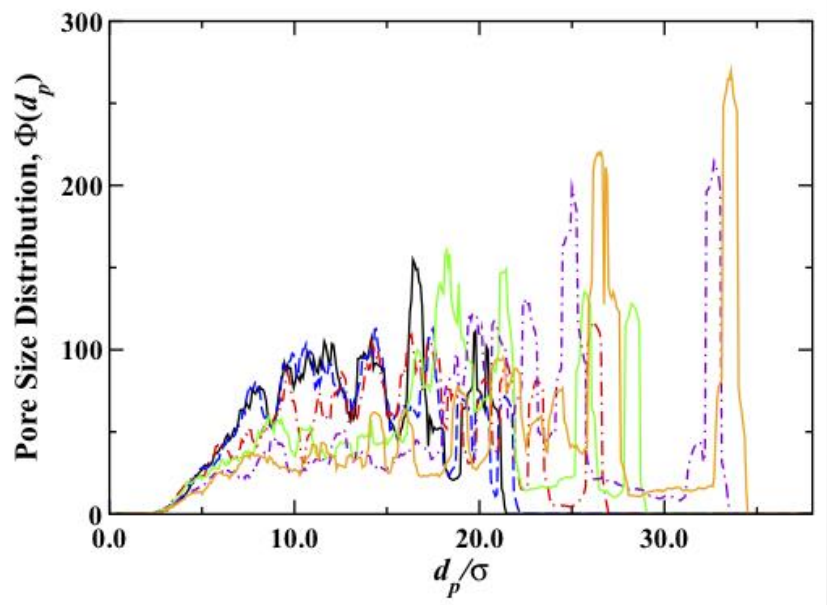

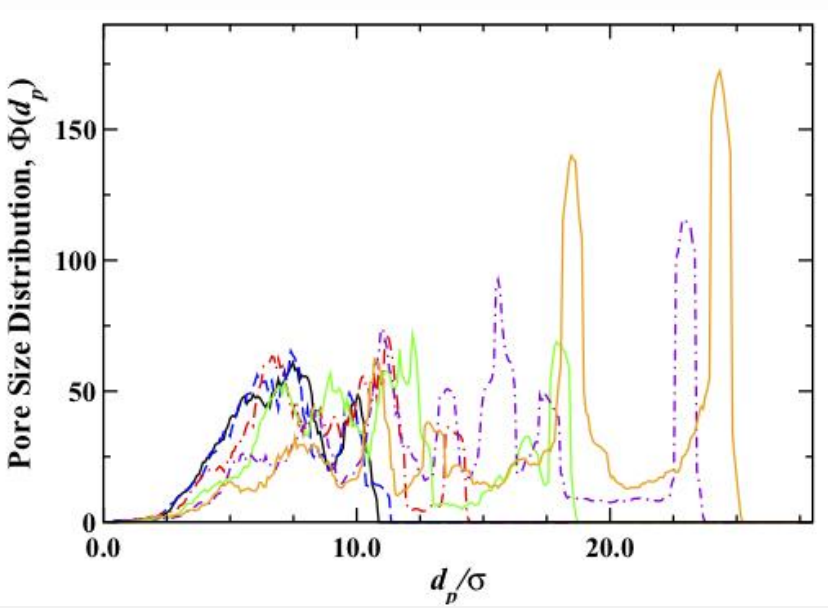

- Small shear causes pore dilations, while largely preserving the shape of the PSDs curves
- At larger strains, peaks corresponding to large pore diameters start to develop
- The number of peaks depends on the average density of the system under consideration
- Small and intermediate pores coalesce into a larger voids
- The scaling is largely preserved in the limit of small and some intermediate pore diameters (narrowing!)

Pore geometry evolution under shear: Density

Pore size distributions, measured at $\rho\sigma^3$ = 0.3 (a), 0.5 (b), and 0.8 (c) are shown at different shear strains.

a)

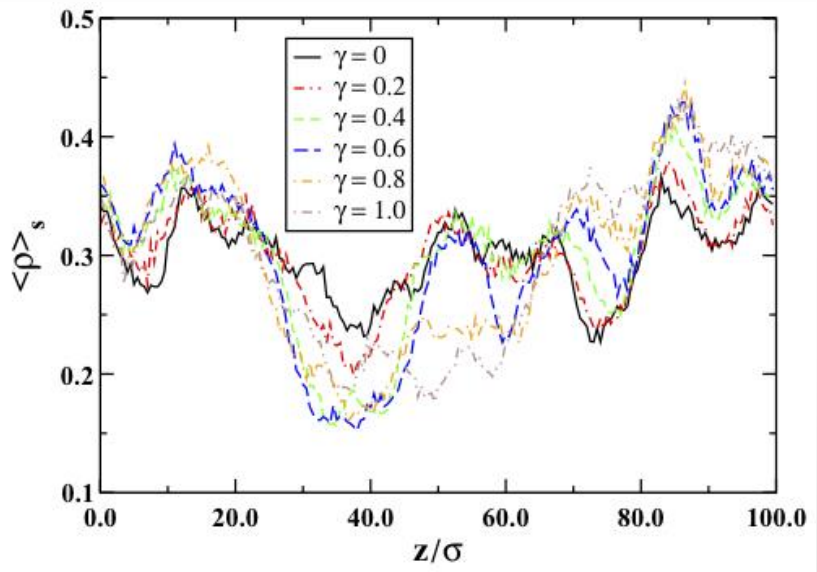

b)

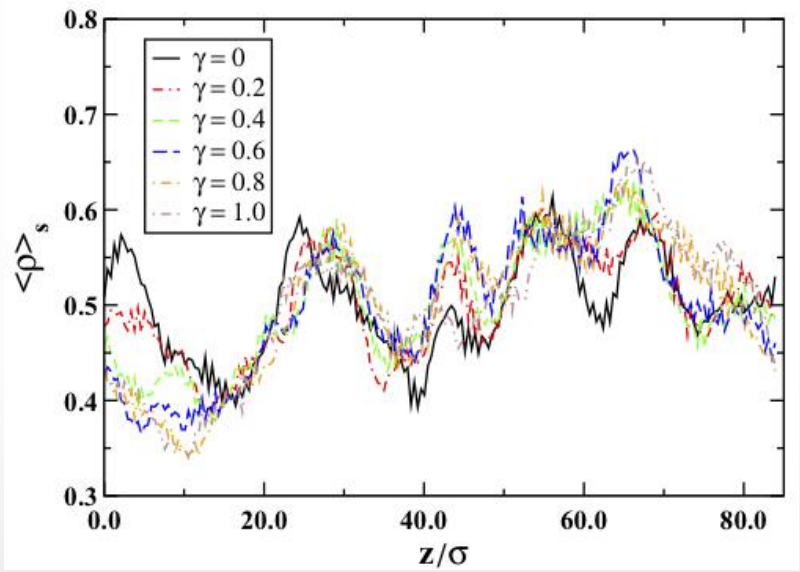

c)

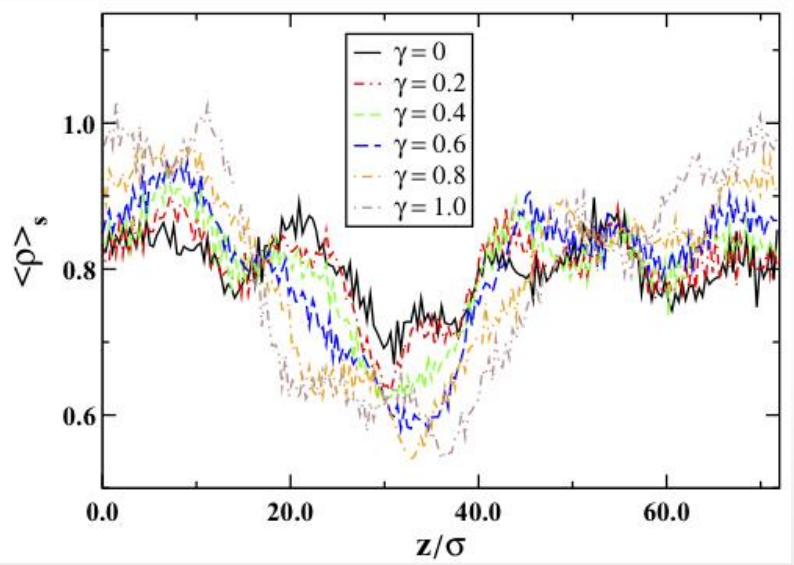

- Materials rearrangement takes place under shear (trivial)
- There are growing pores and regions where voids closure occurs
- The weak spots are defined by the extent of lower density regions
- In a) note: the localized lowest density regions is not a weak spot
- Extent of lower (then the average) density region is the defining factor

Summary and Outlook

- A model of porous materials with varying porosity was studied
- Porosity is varied in a wide range
- Pore size distributions were quantified
- A scaling relation for pore size distributions was deduced
- Effects of the average density and temperature on porosity were investigated
- Density of solid domains was studied as a function of average density
- A scaling relation for porosity variation with average density was derived
- Porous systems responses to mechanical loadings were investigated

- The model systems developed can be used for studies of adsorption in porous materials
- Mechanical effects due to adsorption can readily be investigated using a combination of standard MD and MC methods